AMERICAN ACADEMY OF OPHTHALMOLOGY®

Evaluation of Foveal Cone and Müller Cells in Epiretinal Membrane using Adaptive Optics OCT

Masaharu Ishikura, MD, Yuki Muraoka, MD, PhD, Shin Kadomoto, MD, PhD, Naomi Nishigori, MD, Takahiro Kogo, MD, Shogo Numa, MD, PhD, Eri Nakano, MD, PhD, Masayuki Hata, MD, PhD, Kenji Ishihara, MD, PhD, Sotaro Ooto, MD, PhD, Akitaka Tsujikawa, MD, PhD

Objective: To investigate cellular-level morphological alterations in the retinal neuroglia in eyes with epiretinal membrane (ERM).

Design: Prospective cross-sectional, observational study (November 2020−May 2022).

Subjects and Controls: We included 41 eyes with unilateral idiopathic ERM and 33 healthy eyes of healthy volunteers.

Methods: We examined the foveal microstructures in all eyes using adaptive optics OCT (AO-OCT) with axial and lateral resolutions of 3.4 and 3.0 μm, respectively. Adaptive optics OCT images were acquired for a 2.5° (728 μm) area at the foveal center.

Main Outcome Measures: Foveal microstructures on AO-OCT images, best-corrected visual acuity (BCVA) in logarithm of the minimum angle of resolution units, and associations between these parameters.

Results: Adaptive optics OCT imaging of healthy eyes and eyes with ERM revealed sharp hyperreflective lines of the external limiting membrane (ELM), accompanied by hyporeflective gaps, individual nuclei of the foveal cone photoreceptors, and Müller cell bodies. The arrangement of Müller cell bodies was more vertical in eyes with ERM than in normal eyes. Epiretinal membranes adhered to foveal Müller cells via the internal limiting membrane (ILM), exerting vertical traction that pulled the foveal cones anteriorly. Adaptive optics OCT also enabled visualization of outer segment (OS) discs. Hyperreflective changes in the OS discs were observed beneath the vertically thickened ellipsoid zone (EZ) in 15 eyes (36.6%) with ERM. For eyes with ERM, multiple regression analysis showed that the length from ILM to the inner border of the outer nuclear layer and the EZ thickness were significantly associated with BCVA ($\beta = 5.3 \times 10^{-4}$ and 82.7×10^{-4}, respectively), with associated 95% confidence intervals of 1.3×10^{-4} to 9.3×10^{-4} ($P = 0.011$) and 39.0×10^{-4} to 126.5×10^{-4} ($P < 0.001$), respectively. The EZ thickness was significantly and positively associated with the length from ELM to the retinal pigment epithelium ($\beta = 23.9 \times 10^{-2}$, 95% confidence interval: 4.8×10^{-2} to 42.9×10^{-2}; $P = 0.015$).

Conclusions: Cellular imaging of retinal neuroglia by AO-OCT may suggest possible mechanisms associated with visual impairment in patients with ERM, which could potentially contribute to the growing body of knowledge on its pathophysiology. However, these insights require further validation through extensive studies to fully ascertain their significance.

Financial Disclosure(s): Proprietary or commercial disclosure may be found in the Footnotes and Disclosures at the end of this article. *Ophthalmology Science 2024;4:100362*

Supplemental material available at www.ophthalmologyscience.org.

Epiretinal membrane (ERM) is a common macular disease with a high-prevalence in middle-aged and elderly individuals.[1,2] When macular ERM thickens and distorts the retina, it can cause impaired visual acuity (VA) and metamorphopsia, which often requires macular surgery. When retinal morphological changes are mild, the visual prognosis is good, however, when they are severe, there is limited improvement in vision, even after vitrectomy.[3]

Before observations of the "cotton ball sign"[4] and "bouquet sign"[5] using spectral domain (SD)-OCT were reported, Dupas et al[6] and Pison et al[7] described foveal elevation of the photoreceptor outer segment (OS) at the center of the fovea, which resulted in a foveal yellow spot. They also discussed the role of centripetal contraction of the photoreceptors triggered by contraction of cystoid macular edema, a hypothesis reinforced by the frequent occurrence of micropsias. These findings, together with the signs we observed using SD-OCT,[4–7] contribute to a comprehensive understanding of the changes in the photoreceptor layers in patients with ERM. However, given the limited resolution of SD-OCT, microstructural changes at the cellular level and the complete mechanism by which ERM

https://doi.org/10.1016/j.xops.2023.100362
ISSN 2666-9145/23

impairs the photoreceptors in the outer retina remain to be elucidated.

Adaptive optics (AO) has been studied as a strategy for increasing the resolution and contrast in fundus imaging. In a study using AO-scanning laser ophthalmoscopy (SLO), "microfolds" (multiple thin, straight, hyporeflective lines in the photoreceptor layer) were identified in patients with ERM.[8] However, the 3-dimensional association between ERM and cone photoreceptors cannot be observed because AO-SLO allows observation in a plane parallel to the retina.

Recently, we applied the AO system to OCT imaging and succeeded in visualizing individual photoreceptor nuclei and Müller cells in the human macula. Müller cells are major retinal glia in the human macula, located between the internal limiting membrane (ILM) and external limiting membrane (ELM).[9] The aim of the present study was to examine the microstructural changes in the retinal neuroglia using AO-OCT in order to understand the mechanism by which ERM on the retinal surface damages cone photoreceptors in the outer retina.

Methods

Participants

This prospective, cross-sectional, observational study adhered to the tenets of the Declaration of Helsinki. The institutional review board and ethics committee of Kyoto University Graduate School of Medicine (Kyoto, Japan) approved the study. Written informed consent was obtained from each patient and healthy volunteer prior to any study procedure or examination.

We included 41 eyes of 41 patients (23 men and 18 women) with unilateral idiopathic ERM who visited Kyoto University Hospital between November 2020 and May 2022, in addition to 33 healthy eyes of 33 volunteers (15 men and 18 women) with no history or evidence of systemic or macular diseases, in this study. The diagnosis of idiopathic ERM was based on the presence of fibrocellular tissue at the vitreoretinal interface on SD-OCT (Spectralis HRA + OCT, Heidelberg Engineering) images. The axial and lateral optical resolutions of SD-OCT were 7 and 14 μm, respectively.

We excluded eyes with macular pucker, tractional and degenerative lamellar holes, visually significant cataract, or any potential cause of vision loss other than ERM. Moreover, we excluded eyes with ocular diseases such as keratoconus, high myopia (more severe than −6 diopters), high astigmatism (more severe than ± 3 diopters) as well as those with poor-quality AO-OCT images caused by eye movement or media opacities.

AO-OCT Imaging Protocol

We developed an imaging system (Canon Inc) that could simultaneously capture AO-OCT and SLO images. Correction of the aberrations in the AO system achieved axial and lateral resolutions of 3.4 and 3.0 μm, respectively. Adaptive optics OCT images were acquired for a 2.5° (728 μm) area at the center of the fovea (Figure S1, available at https://www.ophthalmologyscience.org/). The AO-OCT images were scanned for 15 second per retinal area at a rate of 45 frames/s, following which they were averaged using built-in software.

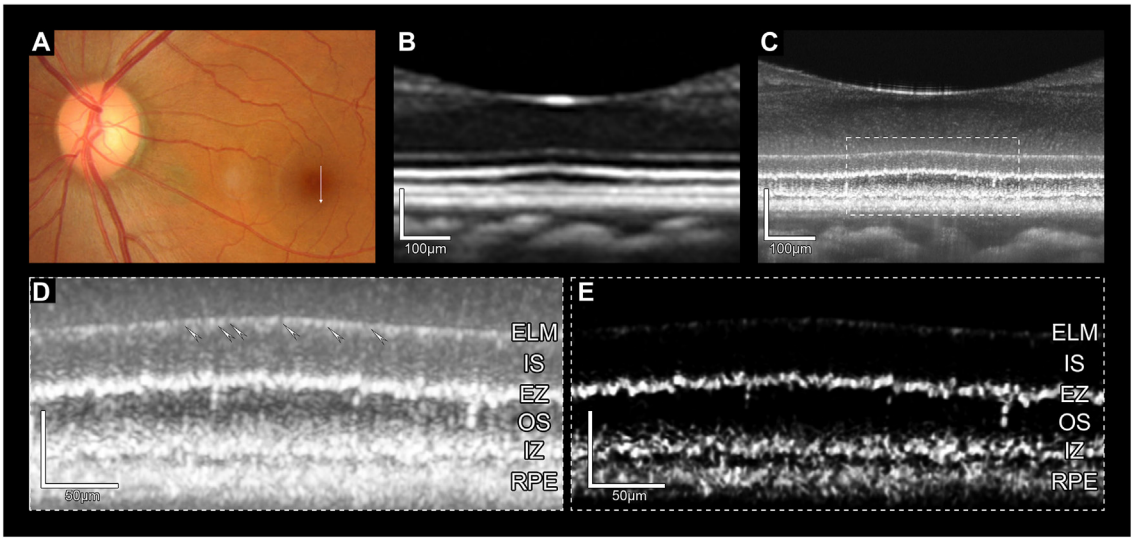

Figure 2. Foveal microstructures in a healthy eye examined by adaptive optics (AO)-OCT. **A,** A color fundus photograph. The arrow shows the vertically sectioned areas (728 μm) for spectral domain (SD)-OCT and AO-OCT (shown in B and C, respectively). **B,** An SD-OCT image of the fovea along the arrow shown in A. The image shows four hyperreflective bands in the outer retina; these are the external limiting membrane (ELM), ellipsoid zone (EZ), interdigitation zone (IZ), and retinal pigment epithelium (RPE) bands. Single retinal neuroglial cells cannot be observed. **C,** An AO-OCT image of the fovea along the arrow shown in **A**. Granules representing the inner segment (IS) and each outer segment (OS) disc in addition to the four hyperreflective bands are visible. **D,** A magnified AO-OCT image of the outer retina surrounded by the dotted square in **C**. ELM is delineated as a sharp, hyperreflective, horizontal line accompanying low reflective gaps at intervals (arrows). EZ is also depicted as a horizontal hyperreflective band formed with clusters of long, spindle-shaped granules. The hyperreflective band is somewhat irregularly straight compared to the ELM line. In the OS area, each disc is stacked vertically. **E,** An AO-OCT image adjusted with gamma correction to enhance EZ visibility in the AO-OCT image. Using a gamma value of 8.5, the image was adjusted to emphasize the EZ, making the long, spindle-shaped, hyperreflective clusters that compose the EZ band more clearly visible. This correction process was performed using the open-source software, ImageJ/FIJI, released on May 30, 2017.

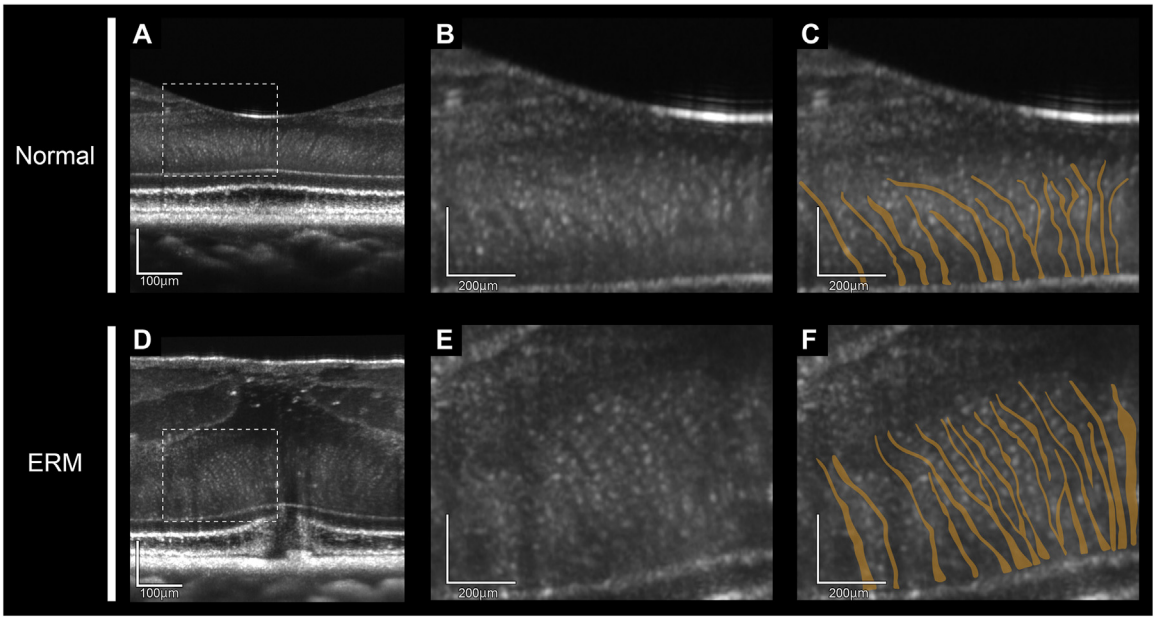

Figure 3. Vertical adaptive optics (AO)-OCT sections. **A,** A vertical AO-OCT image of the fovea of a healthy participant. **B,** A magnified AO-OCT image of the retinal area surrounded by the dotted square in **A**. Each cone nucleus can be observed in the outer nuclear layer (ONL) as a highly reflective dot. Müller cell bodies can be observed in ONL as obliquely arranged thin structures with low reflectivity. **C,** The AO-OCT image in **B** showing the arrangement of Müller cells. The arrangement of Müller cells in ONL is shown by the orange areas. **D,** A vertical AO-OCT image of an eye with epiretinal membrane (ERM). **E,** A magnified AO-OCT image of the retinal area surrounded by the dotted square in **D**. **F,** The AO-OCT image in **E** showing the arrangement of Müller cells. The arrangement of Müller cells in ONL is shown by the orange areas. The Müller cell bodies are arranged more vertically than those in the healthy eye.

Evaluations of the AO-OCT Images

Adaptive optics OCT visualized Müller cell bodies as hyporeflective thin structures in the retina between ILM and ELM (Figures 2 and 3). We evaluated differences in the delineation of structures between SD-OCT and AO-OCT. Using the AO-OCT images, we also compared the cellular structures at the fovea between healthy eyes and eyes with ERM.

We used the AO-OCT images of the foveal center to quantify various parameters, including the length from ILM to the retinal pigment epithelium (RPE), length from ILM to ELM, outer nuclear layer (ONL) thickness, ellipsoid zone (EZ) thickness, and length from ELM to RPE (Figure S1). The ILM and ELM coordinates were identified as the points of peak reflectivity for each membrane (Figure S1). The inner border of ONL, inner and outer borders of EZ, and inner border of RPE were defined as the locations where the maximum and minimum reflectivities of each structure were averaged (Figure S1). The ONL thickness was determined as the distance between the inner border of ONL and ELM, while the EZ thickness was assessed as the full-width half-maximum of EZ (Figure S1). In instances where RPE parameters were measured, we used the coordinate of the inner border of RPE. For eyes with ERM, we examined the association of the EZ thickness with the length from ELM to RPE and the logarithm of the minimum angle of resolution (logMAR) best-corrected VA (BCVA).

We applied a gamma correction process to our AO-OCT images to enhance the visibility of the EZ (Figure 2E). This process was performed with the following formula, Intensity_out = Intensity_in ^ (1/gamma). After normalizing the pixel brightness within a range of 0.0 to 1.0, we applied this formula to reduce the brightness in mid-intensity regions. Consequently, this processing rendered structures other than the EZ less visible, thus emphasizing the EZ. In this study, we used a gamma value of 8.5 to adjust the extent of emphasis on different structures within the image. This correction process was performed using the open-source software, ImageJ/FIJI, released on May 30, 2017.

Statistical Analysis

Statistical analyses were performed using JMP 16 software (SAS Institute Inc). All values are presented as mean ± standard deviation. We converted the decimal BCVA measured using the Landolt chart to logMAR units. Retinal parameters with a normal distribution were compared between normal subjects and patients with ERM using the t test. For comparisons of characteristics between healthy participants and patients with ERM and the analysis of AO-OCT findings for healthy participants and patients with ERM, a 2-sided test was utilized for statistical analyses. A P value of < 0.05 was considered statistically significant. We determined the association of the EZ thickness with the length from ELM to RPE and logMAR BCVA using the Pearson product-moment correlation coefficient. To evaluate the association between each retinal thickness parameter and BCVA, we performed multiple linear regression analysis with a linear model, in which the logMAR BCVA was set as the objective variable and the length from ILM to the inner border of ONL, ONL thickness, EZ thickness, and length from ELM to RPE were set as explanatory variables based on the confirmation that there was no multicollinearity among these explanatory variables.

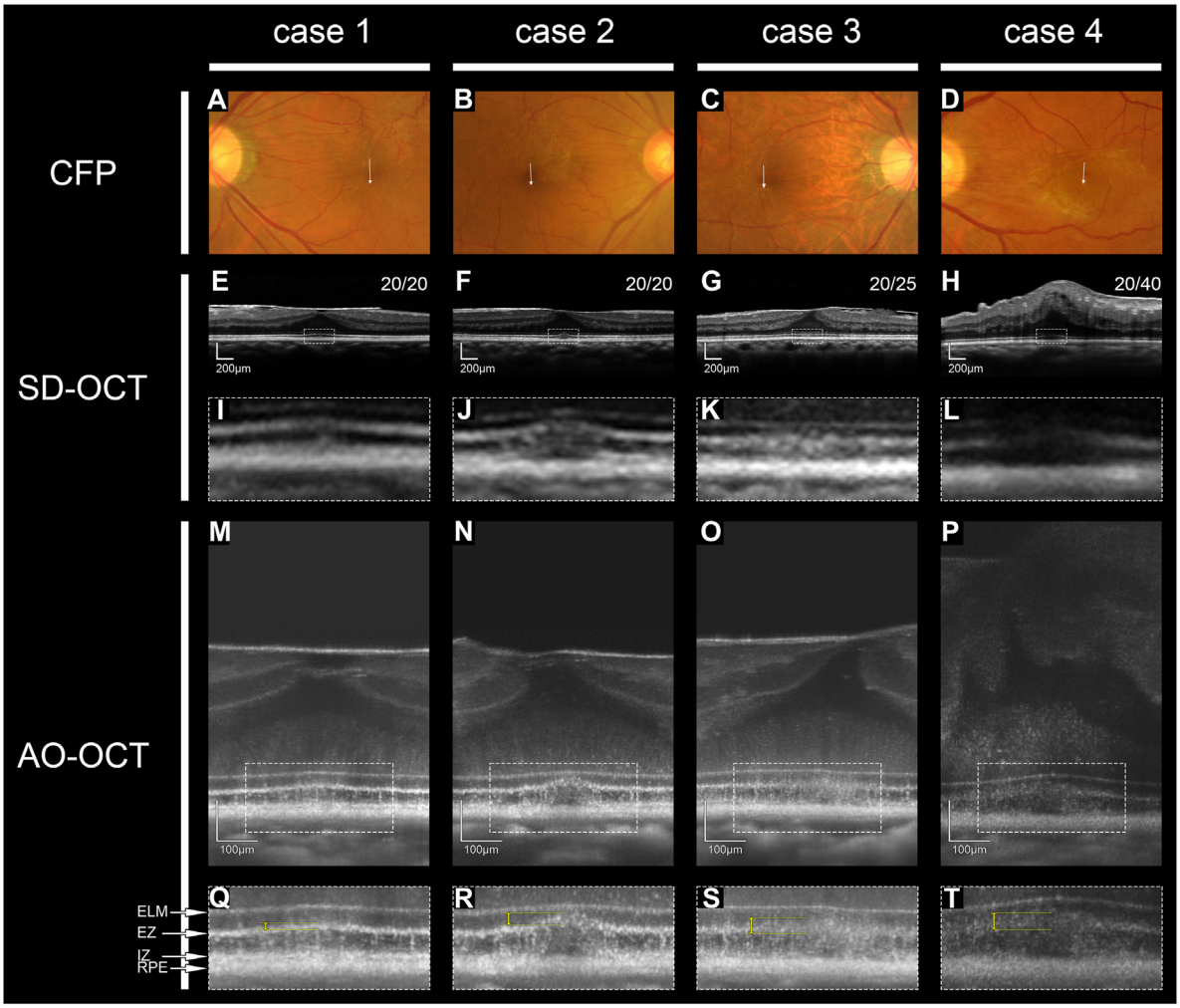

Figure 4. Changes in the ellipsoid zone (EZ) thickness in four cases with epiretinal membrane. Cases 1 to 4 are shown from left to right. The Snellen visual acuity was 20/20 for case 1 (left), 20/20 for case 2 (middle left), 20/25 for case 3 (middle right), and 20/40 for case 4 (right). **A**–**D,** Color fundus photographs (CFP). **E**–**L,** Spectral domain (SD)-OCT images. The images in I–L are magnifications of the areas in the dotted squares in the SD-OCT images in **E**–**H**, respectively. **M**–**T,** Adaptive optics (AO)-OCT images. The images in **Q**–**T** are magnifications of the areas in the dotted squares in the AO-OCT images in **M**–**P**, respectively. The EZ thickness is 18 μm for case 1, 30 μm for case 2, 39 μm for case 3, and 42 μm for case 4. In the SD-OCT image of case 4 (L), the EZ line appears disrupted. In contrast, EZ is less reflective and vertically thickened on the AO-OCT image (T). ELM = external limiting membrane; IZ = interdigitation zone; RPE = retinal pigment epithelium.

Among the explanatory variables, continuous variables were standardized to a mean of 0 and a variance of 1.

Results

Table 1 shows the background characteristics of the study participants. There were no significant differences in sex, mean age, spherical equivalent, and axial length between the healthy participants and patients with ERM (Table 1).

Spectral domain OCT images of healthy eyes showed 4 hyperreflective bands in the outer retina: ELM, EZ, interdigitate zone, and RPE. However, individual retinal neuroglial cells could not be distinguished (Figure 2). Adaptive optics OCT images of both healthy eyes and eyes with ERM clearly visualized ELM as a sharp hyperreflective line accompanied by hyporeflective gaps at intervals (Figure 2). Furthermore, they displayed each foveal cone nucleus in ONL as a highly reflective dot and each Müller cell body as a hyporeflective thin structure in the retina between ILM and ELM (Figures 2 and 3). Müller cell bodies in healthy eyes were arranged vertically at the foveola and diagonally outside the foveola, whereas those in eyes with ERM were arranged more vertically, even outside the foveola (Figure 3).

Ellipsoid zone was observed as a highly reflective band on SD-OCT images. However, on AO-OCT images of healthy eyes, each ellipsoid that made up the band was arranged in a single row or a few rows in the horizontal direction (Figure 2). In eyes with ERM, ERM adhered to foveal Müller cells via ILM and exerted vertical traction that pulled the foveal cones toward the inner retina (Figure 4). On SD-OCT images, the EZ band appeared partially disrupted, whereas on AO-OCT images of the

Table 1. Characteristics of Healthy Participants and Patients with Idiopathic ERM

	Healthy Participants	Patients with ERM	*P* Value
Number (men/women)	33 (15/18)	41 (23/18)	(0.36)*
Number, eyes	33	41	n.a.
Age, years	68.2 ± 10.3	68.2 ± 8.2	0.99**
Spherical equivalent, diopter	−1.2 ± 1.6	−0.9 ± 1.4	0.44**
Axial length, mm	24.2 ± 1.3	24.7 ± 1.4	0.21**
logMAR visual acuity	−0.05 ± 0.07	0.06 ± 0.13	< 0.001**
Snellen visual acuity, range	20/20−20/13	20/50−20/13	n.a.
Intraocular pressure, mmHg	13.6 ± 2.5	13.7 ± 1.8	0.86**

ERM = epiretinal membrane; logMAR = logarithm of the minimum angle of resolution; n.a. = not applicable.
The data are shown as mean ± standard deviation unless otherwise indicated.
*Sex differences between healthy participants and patients with idiopathic ERM were assessed using the chi-square test.
**Systemic factors were compared between healthy participants and patients with idiopathic ERM using the t test for parameters with normal distribution.

corresponding area, the EZ band was not disrupted and appeared vertically thickened (Figure 4).

The OS discs could not be delineated by SD-OCT; however, they were delineated by AO-OCT in both healthy eyes and eyes with ERM (Figures 2 and 3). In 15 (36.6%) eyes with ERM, the OS discs became more hyperreflective immediately beneath the vertically thickened EZ (Figure 4). The hyperreflective change in the OS discs on AO-OCT images was occasionally accompanied by the cotton ball sign, a hyperreflective finding in the outer portion of the photoreceptor layers of fovea with ERM, on SD-OCT images (Figure 4).

Table 2 shows the results of quantitative evaluations of the foveal structures using AO-OCT. The whole retinal thickness, length from ILM to the inner border of ONL, ONL thickness, EZ thickness, and length from ELM to RPE were significantly greater in eyes with ERM than in healthy eyes (Table 2, Figure 3). Multiple regression analysis showed that the length from ILM to the inner border of ONL and the EZ thickness were significantly associated with the logMAR BCVA ($\beta = 5.3 \times 10^{-4}$, 82.7×10^{-4}, respectively), with associated 95% confidence intervals of 1.3×10^{-4} to 9.3×10^{-4} ($P = 0.011$) and 39.0×10^{-4} to 126.5×10^{-4} ($P < 0.001$), respectively (Table 3). The EZ thickness was significantly and positively associated with the length from ELM to RPE ($\beta = 23.9 \times 10^{-2}$, 95% confidence interval = 4.8×10^{-2} to 42.9×10^{-2}, $P = 0.015$).

Discussion

In the present study, we utilized AO-OCT to examine the retinal microstructures in eyes with idiopathic ERM and compared the findings with those for healthy eyes as well as those of SD-OCT.

Idiopathic ERM is characterized by fibrotic proliferation in the vitreous cortex,[10,11] which can cause shrinkage due to fibrotic remodeling.[12] Previous studies using SD-OCT have reported that the status of the foveal EZ is strongly associated with visual function in various macular diseases, including ERM, and they have identified photoreceptor-associated findings such as the cotton ball[5] and bouquet signs[4] and acquired vitelliform lesions.[13] These findings suggest that ERM has a significant impact on foveal cones in the outer retina; however, the underlying cellular mechanisms are not fully understood.

The use of AO technology has enabled the observation of retinal microstructures, which is not feasible with conventional imaging.[14,15] Adaptive optics SLO has been used to identify microfolds in the photoreceptor layer in eyes with ERM; however, these folds might simply be projections of wrinkles in the inner retina onto the photoreceptor layer. Recently, AO technology was also applied for OCT imaging, and our previous study using AO-OCT revealed the cellular structure of foveal cones and Müller cells, which could not be delineated by SD-OCT, in healthy eyes.[9] In the present study, we utilized AO-OCT to examine the foveal microstructures in eyes with ERM and found that Müller cells could be visualized as hyporeflective, single cell bodies penetrating ONL and the outer plexiform layer in both healthy eyes and eyes with ERM (Figures 2 and 3). This finding suggests that the difference in depth and lateral resolution may explain the difference in the delineation of retinal neuroglia between SD-OCT and AO-OCT.

Müller cells are primary retinal glial cells and are involved in the maintenance of structural stability within the retina.[16] In addition, they play a critical role in the maintenance of molecular homeostasis by degrading neurotransmitters.[16,17] Histologically, Müller cells at the fovea run in a direction that is vertical to oblique, in relation to the retinal plane, whereas those outside the foveola pass through Henle's fiber layer and travel in a vertical to oblique direction and then in a vertical direction, thus forming a Z-shape.[18,19] Adaptive optics OCT images of the healthy eyes in the present study revealed that the alignment of Müller cells (Figure 3) was similar to that observed in histological examination in a previous study.[19] However, Müller cells outside the foveola were arranged more vertically in eyes with ERM than in healthy eyes (Figure 3). The traction force of ERM parallel to the retinal plane has been assessed by analysis of the depth of serrated wrinkles,[20] deviation of retinal vessels,[21] ectopic inner foveal layer,[22] and reduced size of the foveal avascular zone.[23] These findings suggest that afferent contraction at the retinal surface may alter the horizontal alignment of foveal Müller cells. The AO-OCT findings in the present study support the speculation based on previous SD-OCT findings.[20–23]

In the present study, AO-OCT showed that ERM adhered to the basement membrane of Müller cells (ILM) and anteriorly pulled the Müller cells and the photoreceptors that contacted the deep edge of the Müller cells (Figures 3 and 4). Histologically, the area from ELM to the deep edge of EZ is

Table 2. Findings of Adaptive Optics OCT for Healthy Participants and Patients with ERM

	Healthy Participants	Patients with ERM	*P* Value
Whole retinal thickness (μm)	193.6 ± 26.1	420.7 ± 98.8	< 0.001*
Length from ILM to the inner edge of ONL (μm)	41.2 ± 15.2	208.6 ± 95.9	< 0.001*
ONL thickness (μm)	74.9 ± 12.6	124.0 ± 16.7	< 0.001*
EZ thickness (μm)	9.8 ± 1.25	19.6 ± 8.7	< 0.001*
Length from ELM to RPE (μm)	77.5 ± 7.5	88.0 ± 14.5	< 0.001*

ELM = external limiting membrane; ERM = epiretinal membrane; EZ = ellipsoid zone; ILM = internal limiting membrane; ONL = outer nuclear layer; RPE = retinal pigment epithelium.
The data are shown as mean ± standard deviation unless otherwise indicated.
*Each retinal thickness parameter was compared between healthy participants and patients with ERM using the t test for parameters with normal distribution.

the photoreceptor inner segment (IS).[24] Although interpretation of the OCT section that corresponds to the IS/OS boundary remains debatable,[25] recent research has suggested that it represents the region inside IS that is rich in mitochondria.[24] On AO-OCT imaging, EZ in healthy eyes appeared as a highly reflective band parallel to the retinal plane, containing a single ellipsoid in the horizontal direction (Figure 2). However, in some eyes with ERM, the highly reflective area of the ellipsoid became broader anteriorly (Figure 4 and Table 2), and the laterally adjacent ellipsoids could not be distinguished as separate structures (Figure 4).

In the present study, poor BCVA was associated with vertical thickening of EZ and an increase in length from ILM to the inner border of ONL (Table 3). In addition, vertical thickening of EZ was positively associated with the distance from ELM to RPE (Table 4). Müller cells attach to the photoreceptor IS via tight junctions.[26–28] The associations observed in the present study suggest that morphological changes in the foveal cone and Müller cells are closely linked to the dysfunction of cone photoreceptors. Müller cells might exert traction on the cone IS and potentially alter the distribution or dynamics of mitochondria inside IS.[29] We consider AO-OCT to be the imaging modality that can facilitate noninvasive visualization of mitochondria in vivo, with the photoreceptor IS being the rare location in the human body where this could be possible.

The area between EZ and interdigitate zone on OCT is consistent with the area of OS discs, which are rich in visual pigments, on histological sections.[30,31] In the present study, AO-OCT also allowed evaluation of the cone OS (Figures 2–4). In healthy eyes, the OS area could be observed as a stack of moderately hyperreflective discs, perpendicular to the retinal plane. In 36.6% eyes with ERM, the OS discs were more hyperreflective just beneath the vertically thickened EZ (Figure 4); this could indicate that the damage to the foveal cones was affected by identical Müller cells. The hyperreflective change in the OS discs on AO-OCT was occasionally accompanied by the cotton ball sign on SD-OCT; this suggests that the cotton ball sign is partially common to hyperreflective OS discs. However, the cotton ball sign was sometimes not evident in the area with the hyperreflective change in the OS discs (Figure 4). We speculate that the hyperreflective change in the OS discs is an indication of stress on the cone photoreceptors even before appearance of the cotton ball sign; thus, it has potential as a novel early biomarker of cone photoreceptor damage in eyes with ERM.

This study has several limitations. First, the analysis was purely cross-sectional, thus limiting our understanding of the longitudinal effects of ERM on retinal neuroglia based on AO-OCT data. In addition, our focus was on the cone cells in ONL and Müller cells; this may have caused us to overlook the potential visibility and relevance of bipolar and ganglion cells. Second, postoperative changes in the retinal structures remain unclear. This lack of clarity extends to the identification of Müller cells, which was based on established literature and the known anatomy and orientation of

Table 3. Multiple Regression Analyses to Determine the Association between Retinal Structures Examined using Adaptive Optics OCT and the Best-Corrected Visual Acuity (Logarithm of the Minimum Angle of Resolution Units)

	β ($\times 10^{-4}$) (95% Confidence Interval)	Standard β ($\times 10^{-2}$) (95% Confidence Interval)	*P* Value
Length from ILM to the inner edge of ONL (μm)	5.3 (1.3–9.3)	39.4 (9.5–68.2)	0.011
ONL thickness (μm)	−9.4 (−32.2–13.3)	−12.1 (−41.2–17.0)	0.40
EZ thickness (μm)	82.7 (39.0–126.5)	55.4 (26.1–84.7)	< 0.001
Length from ELM to RPE (μm)	−8.4 (−35.5–18.7)	−9.3 (−39.4–20.8)	0.54

The data are shown as mean ± standard deviation unless otherwise indicated.
ELM = external limiting membrane; EZ = ellipsoid zone; ILM = internal limiting membrane; ONL = outer nuclear layer; RPE = retinal pigment epithelium.

Table 4. Multiple Regression Analyses to Determine the Association between Retinal Structures Examined using Adaptive Optics OCT and the Ellipsoid Zone Thickness

	β ($\times 10^{-2}$) (95% Confidence Interval)	Standard β ($\times 10^{-2}$) (95% Confidence Interval)	*P* Value
Length from ILM to the inner edge of ONL (μm)	0.4 (−2.6–3.5)	−4.6 (−28.7–38.0)	0.78
ONL thickness (μm)	15.7 (−0.8–32.2)	30.0 (−1.6–61.6)	0.062
Length from ELM to RPE (μm)	23.9 (4.8–42.9)	39.6 (8.0–71.2)	0.015

The data are shown as mean ± standard deviation unless otherwise indicated.
ELM = external limiting membrane; ILM = internal limiting membrane; ONL = outer nuclear layer, RPE = retinal pigment epithelium.

these cells within the retina. Given their long, radial orientation spanning the full thickness of the retina, we are confident about our interpretation. However, we acknowledge that AO-OCT may not definitively distinguish between Müller cells and other retinal structures. Last, while Govetto et al suggested that acquired vitelliform lesions might follow the bouquet sign,[4] this hypothesis could not be confirmed in our study because we did not observe any patients with acquired vitelliform lesions. This also means that we could not confirm the hypothesized role of the bouquet sign in the development of these lesions.

Conclusions

While AO-OCT provided remarkably detailed observations of retinal changes in ERM, the clinical significance of these findings requires further study. It should be noted that in similar cases, Pison et al found that preoperative VA was lower in cases with EZ elevation,[7] whereas there was no difference in the postoperative results. This underscores the need for future investigations to evaluate the correlation between these detailed AO-OCT observations and both preoperative and postoperative VA. We posit that the vertical thickening of the foveal EZ could serve as an early biomarker of mitochondrial damage in cone photoreceptors. However, to confirm our findings and explore their potential clinical implications, studies comparing pre and postoperative AO-OCT findings and investigating the natural history of the disease are warranted. Furthermore, comparison of AO-OCT and histological findings in animal models of ERM would provide valuable additional insights.

Footnotes and Disclosures

Originally received: May 3, 2023.
Final revision: June 24, 2023.
Accepted: June 26, 2023.
Available online: July 4, 2023. Manuscript no. XOPS-D-23-00090.

Department of Ophthalmology and Visual Sciences, Kyoto University Graduate School of Medicine, Kyoto, Japan.

Disclosures:

All authors have completed and submitted the ICMJE disclosures form.

The authors made the following disclosures. Y.M.: Grant and Financial support − Rohto Pharmaceutical, Novartis Pharma, Santen Pharmaceutical, Senju Pharmaceutical, AMO Japan, HOYA, Johnson & Johnson KK, Bayer Yakuhin, Alcon Japan, Canon.

S.K.: Grant support − Canon, NIDEK Co, LTD.

S.N.: Grant support − Senju Pharmaceutical, Kowa Pharmaceutical, Santen Pharmaceutical.

E.N.: Grant support − Senju Pharmaceutical.

M.H.: Grant and Financial Support − Novartis Pharma, Senju Pharmaceutical, Kyoto Drug Discovery & Development Patent.

S.O.: Grant support − Bayer Yakuhin, Kowa Pharmaceutical, Janssen Pharmaceutical, Novartis Pharma, AMO Japan, Santen Pharmaceutical, Alcon Japan, Senju Pharmaceutical.

A.T.: Grant and Financial support − Canon, Kowa Pharmaceutical, Pfizer, Wakamoto Pharmaceutical, Nitten Pharmaceutical, AbbVie GK, Senju Pharmaceutical, Otsuka Pharmaceutical, Findex, Santen Pharmaceutical, AMO Japan, Alcon Pharma; Consultant − Bayer Yakuhin, Novartis Pharma.

This work was supported in part by Canon Inc. (Tokyo, Japan), Rohto Pharmaceutical (Osaka, Japan), and Alcon Japan, Ltd. (Tokyo, Japan). The sponsor or funding organization had no role in the design or conduct of this research.

HUMAN SUBJECTS: This prospective, cross-sectional, observational study adhered to the tenets of the Declaration of Helsinki and institutional review board and ethics committee of Kyoto University Graduate School of Medicine (Kyoto, Japan) approval was obtained. Written informed consent was obtained from each patient and healthy volunteer prior to any study procedure or examination No animal subjects were included in this study.

Author Contribution:

Conception and design: Ishikura, Muraoka, Tsujikawa

Analysis and interpretation: Ishikura, Muraoka, Kadomoto, Nishigori, Kogo, Numa, Nakano, Hata, Ishihara, Ooto, Tsujikawa

Data collection: Ishikura, Muraoka

Obtained funding: N/A; Study was performed as part of regular employment duties at Kyoto university hospital. No additional funding was provided.

Overall responsibility: Ishikura, Muraoka, Hata, Tsujikawa

Abbreviations:
AO = adaptive optics; **BCVA** = best-corrected visual acuity; **ELM** = external limiting membrane; **ERM** = epiretinal membrane; **EZ** = ellipsoid zone; **ILM** = internal limiting membrane; **IS** = inner segment; **logMAR** = logarithm of the minimum angle of resolution; **ONL** = outer nuclear layer; **OS** = outer segment; **RPE** = retinal pigment epithelium; **SD-OCT** = spectral domain OCT; **SLO** = scanning laser ophthalmoscopy; **VA** = visual acuity.

Keywords:
Epiretinal membrane, Adaptive optics, Adaptive optics optical coherence tomography, Müller cell, Ellipsoid zone.

Correspondence:
Yuki Muraoka, MD, PhD, Department of Ophthalmology, Kyoto University Graduate School of Medicine, Sakyo-ku, Kyoto 606-8507, Japan. E-mail: muraoka@kuhp.kyoto-u.ac.jp.

References

1. Ng CH, Cheung N, Wang JJ, et al. Prevalence and risk factors for epiretinal membranes in a multi-ethnic United States population. *Ophthalmol Times*. 2011;118:694−699.
2. Miyazaki M, Nakamura H, Kubo M, et al. Prevalence and risk factors for epiretinal membranes in a Japanese population: the Hisayama study. *Graefes Arch Clin Exp Ophthalmol*. 2003;241:642−646.
3. Asaria R, Garnham L, Gregor ZJ, Sloper JJ. A prospective study of binocular visual function before and after successful surgery to remove a unilateral epiretinal membrane. *Ophthalmol Times*. 2008;115:1930−1937.
4. Govetto A, Bhavsar KV, Virgili G, et al. Tractional abnormalities of the central foveal bouquet in epiretinal membranes: clinical spectrum and pathophysiological perspectives. *Am J Ophthalmol*. 2017;184:167−180.
5. Tsunoda K, Watanabe K, Akiyama K, et al. Highly reflective foveal region in optical coherence tomography in eyes with vitreomacular traction or epiretinal membrane. *Ophthalmol Times*. 2012;119:581−587.
6. Dupas B, Tadayoni R, Erginay A, et al. Subfoveal deposits secondary to idiopathic epiretinal membranes. *Ophthalmol Times*. 2009;116:1794−1798.
7. Pison A, Dupas B, Couturier A, et al. Evolution of subfoveal detachments secondary to idiopathic epiretinal membranes after surgery. *Ophthalmol Times*. 2016;123:583−589.
8. Ooto S, Hangai M, Takayama K, et al. High-resolution imaging of the photoreceptor layer in epiretinal membrane using adaptive optics scanning laser ophthalmoscopy. *Ophthalmology*. 2011;118:873−881.
9. Kadomoto S, Muraoka Y, Uji A, et al. Human foveal cone and Müller cells examined by adaptive optics optical coherence tomography. *Transl Vis Sci Technol*. 2021;10:17.
10. Kritzenberger M, Junglas B, Framme C, et al. Different collagen types define two types of idiopathic epiretinal membranes. *Histopathology*. 2011;58:953−965.
11. Snead DR, Cullen N, James S, et al. Hyperconvolution of the inner limiting membrane in vitreomaculopathies. *Graefes Arch Clin Exp Ophthalmol*. 2004;242:853−862.
12. Kohno RI, Hata Y, Kawahara S, et al. Possible contribution of hyalocytes to idiopathic epiretinal membrane formation and its contraction. *Br J Ophthalmol*. 2009;93:1020−1026.
13. Freund KB, Laud K, Lima LH, et al. Acquired vitelliform lesions: correlation of clinical findings and multiple imaging analyses. *Retina*. 2011;31:13−25.
14. Ishikura M, Muraoka Y, Kadomoto S, et al. Retinal arterial macroaneurysm rupture caused by dissection-like change in the vessel wall. *Am J Ophthalmol Case Rep*. 2022;25:101346.
15. Williams DR, Burns SA, Miller DT, Roorda A. Evolution of adaptive optics retinal imaging [Invited]. *Biomed Opt Express*. 2023;14:1307−1338.
16. Newman E, Reichenbach A. The Müller cell: a functional element of the retina. *Trends Neurosci*. 1996;19:307−312.
17. Bringmann A, Pannicke T, Grosche J, et al. Müller cells in the healthy and diseased retina. *Prog Retin Eye Res*. 2006;25:397−424.
18. Gass JD. Müller cell cone, an overlooked part of the anatomy of the fovea centralis: hypotheses concerning its role in the pathogenesis of macular hole and foveomacualr retinoschisis. *Arch Ophthalmol*. 1999;117:821−823.
19. Yamada E. Some structural features of the fovea centralis in the human retina. *Arch Ophthalmol*. 1969;82:151−159.
20. Kanzaki Y, Doi S, Matoba R, et al. Objective and quantitative estimation of the optimal timing for epiretinal membrane surgery on the basis of metamorphopsia. *Retina*. 2022;42:704−711.
21. Ichikawa Y, Imamura Y, Ishida M. Inner nuclear layer thickness, a biomarker of metamorphopsia in epiretinal membrane, correlates with tangential retinal displacement. *Am J Ophthalmol*. 2018;193:20−27.
22. Govetto A, Lalane 3rd RA, Sarraf D, et al. Insights into epiretinal membranes: presence of ectopic inner foveal layers and a new optical coherence tomography staging scheme. *Am J Ophthalmol*. 2017;175:99−113.
23. Kumagai K, Furukawa M, Suetsugu T, Ogino N. Foveal avascular zone area after internal limiting membrane peeling for epiretinal membrane and macular hole compared with that of fellow eyes and healthy controls. *Retina*. 2018;38:1786−1794.
24. Spaide RF, Curcio CA. Anatomical correlates to the bands seen in the outer retina by optical coherence tomography: literature review and model. *Retina*. 2011;31:1609−1619.
25. Huang Y, Cideciyan AV, Papastergiou GI, et al. Relation of optical coherence tomography to microanatomy in normal and rd chickens. *Invest Ophthalmol Vis Sci*. 1998;39:2405−2416.
26. Heegaard S, Jensen OA, Prause JU. Structure and composition of the inner limiting membrane of the retina. SEM on frozen resin-cracked and enzyme-digested retinas of Macaca mulatta. *Graefes Arch Clin Exp Ophthalmol*. 1986;224:355−360.
27. Daniele LL, Adams RH, Durante DE, et al. Novel distribution of junctional adhesion molecule-C in the neural retina and retinal pigment epithelium. *J Comp Neurol*. 2007;505:166−176.
28. Omri S, Omri B, Savoldelli M, et al. The outer limiting membrane (OLM) revisited: clinical implications. *Clin Ophthalmol*. 2010;4:183−195.
29. McLeod D, Marshall J, Kohner EM, Bird AC. The role of axoplasmic transport in the pathogenesis of retinal cotton-wool spots. *Br J Ophthalmol*. 1977;61:177−191.
30. Sjöstrand FS, Kreman M. Molecular structure of outer segment disks in photoreceptor cells. *J Ultrastruct Res*. 1978;65:195−226.
31. Stone J, van Driel D, Valter K, et al. The locations of mitochondria in mammalian photoreceptors: relation to retinal vasculature. *Brain Res*. 2008;1189:58−69.